JOURNAL OF SOLID STATE CHEMISTRY 38, 342–359 (1981)

Polaron Interaction Energies in Reduced Tungsten Trioxide

E. IGUCHI

Department of Metallurgical Engineering, Yokohama National University, Tokiwadai 156, Hodogaya-ku, Yokohama, 240 Japan

E. SALJE

Mineralogisches Institut der Universität Hannover, Welfengarten 1, D-3000 Hannover, West Germany

AND R. J. D. TILLEY

School of Materials Science, University of Bradford, Bradford BD7 1DP, West Yorkshire, U.K.

Received September 23, 1980; in revised form January 19, 1981

Consideration of the properties of reduced tungsten trioxide suggest that the mobile charge carriers are polarons. As it is uncertain how the presence of polarons will influence the microstructures of the crystallographic shear (*CS*) planes present in reduced tungsten trioxide we have calculated both the polaron–*CS* plane and polaron–polaron interaction energy for a variety of circumstances. Three *CS* plane geometries were considered, {102}, {103}, and {001} *CS* plane arrays, and the nominal compositions of the crystals ranged from $WO_{2.70}$ to $WO_{3.0}$. The polarons were assumed to have radii from 0.6 to 1.0 nm and the polaron–*CS* plane electrostatic interaction was assumed to be screened. The results suggest that for the most part the total interaction energy is small and is unlikely to be of major importance in controlling the microstructures found in *CS* planes. However, at very high polaron densities the interaction energy could be appreciable and may have some influence on the existence range of *CS* phases.

Introduction

Since the discovery that the reduction of WO_3 resulted in the formation of crystallographic shear (*CS*) planes there have been a number of investigations aimed at understanding this behavior. As part of this, some effort has been put into trying to determine *CS* formation energy and to quantify the interactions between *CS* planes in WO_3-like structures (*1–5*). These calculations have shown that while removal of oxygen from the crystal and interactions between the closely spaced atoms within the *CS* planes make up the largest part of the formation energy of these defects, the orientation that they take up seems largely to be influenced by the elastic strain field in the matrix surrounding the *CS* planes and the relaxation of the atoms in the *CS* planes due to this elastic strain field.

In addition to these chemical and mechanical terms, electronic interactions are also likely to be of importance in these systems. In view of this, the electrostatic interaction between *CS* planes was also

0022-4596/81/090342-18$02.00/0

calculated (*6*). In this study, the *CS* phases were considered to be ionic, and the charge imbalance created in the WO_3 structure upon reduction was assumed to be taken up by the creation of W^{5+} or W^{4+} ions which were taken as localized in the *CS* planes themselves. The matrix between the *CS* planes then contained only octahedrally coordinated W^{6+} ions. In terms of this model the electrostatic interactions were found to be small, and of much less importance than the elastic strain energies previously calculated.

Although this simple electrostatic model is useful for describing some features of the *CS* formation, it is at variance with some of the more recently reported properties of the reduced crystals. For example, they possess rather high electrical conductivity and effective dielectric constants at room temperature, show considerable charge carrier concentrations in Hall experiments, and strong quasi-free-carrier absorption in the near-infrared region. These results indicate that mobile charge carriers exist in the reduced phases and have been interpreted in terms of polarons rather than free electrons (*7–12*). It can be anticipated that the presence of an appreciable polaron density may well act so as to shield the *CS* planes from each other, thus reducing electrostatic interactions, while the polarons may well interact with *CS* planes themselves. It is not apparent in an *a priori* fashion how these interactions will influence *CS* plane microstructures, particularly *vis a vis* elastic strain energy, and so we have made quantitative estimates of the appropriate interaction energies. We present the results of these calculations in this paper.

Theoretical Considerations

1. The Nature of the Charge Carriers in WO_{3-x}

Although the crystallographic changes which take place when WO_3 is slightly reduced are fairly well known (*1, 2*) the electronic nature of these reduced oxides is less easy to define. Recent studies have suggested, though, that in the *CS* phases with overall compositions down to about $WO_{2.90}$ only W^{6+} and W^{5+} states are present (*13*). The results of optical and electrical experiments show that in slightly reduced tungsten oxides the charge carrier concentration is identical to the oxygen deficit with two elementary charges present per missing oxygen atom (*14*), and that the charge carriers are highly mobile (*7*). This indicates that they move predominantly in the WO_3-like regions between *CS* planes, for if they were restricted to the *CS* planes we would expect carrier localization and low electronic conductivity. In particular, an ionic model in which the W^{5+} cations are completely immobilized in the *CS* planes is unrealistic and does not accord with the experimental observations.

Having established the presence of highly mobile charge carriers in the tungsten oxide *CS* phases, it is necessary to determine whether the material behaves as a metal, with the carrier wave function fully extended throughout the WO_3-like matrix or whether the carriers are localized as in hopping materials. From ESCA experiments (*15*) it is known that as long as the crystallinity of the matrix is not drastically destroyed, only W^{5+} states appear, but no plasmons occur as are found in the metallic tungsten bronzes. Furthermore, optical experiments show a characteristic absorption near 0.82 eV, similar to the polaronic absorption in WO_3 (*11*). These results, taken together, suggest that the carrier is self-trapped at a tungsten position as a polaron of small or intermediate size.

In the sense of this paper, each of these polarons can be envisaged as an electron surrounded by a locally deformed lattice, which tends to move with the carrier. If the interaction is strong so that local deforma-

tions are large, the resultant charge carrier plus deformation is termed a small polaron, while if the electronic movement is only slightly impeded due to relatively weak interactions with the lattice, it is termed a large polaron. In reduced WO_3 there is some evidence to suggest that at higher temperatures we have large polaron behavior, while at lower temperatures this may change to small polaron behavior.

The deformed region around the polaron also leads us to a concept of a polaron radius associated with these mobile charge carriers. This notion is important, as it allows us to obtain a quantitative idea of the highest possible carrier densities one can obtain in a crystal and also to estimate in a more qualitative way the lower stability limit of a particular *CS* series. We will return to this latter point in the discussion.

The outcome of these considerations is to suggest that a reasonable model which accounts for the electrical properties of the WO_{3-x} *CS* phases is one in which the excess charges created when WO_3 is reduced are divided into two groups. We will have a polaron population between the *CS* planes which can be regarded as W^{6+} ions with trapped electrons to generate W^{5+} states. The balance of the charges will be localized in the *CS* planes themselves, again in the form of W^{5+} ions. If we assume that all of the W^{5+} states are to be found between the *CS* planes, then the *CS* planes will act as positively charged, electrically rather isolating planar faults containing only W^{6+} ions, in a negatively charged WO_3 matrix. As we imagine W^{5+} states to be transferred from the inter-*CS* plane region into the CS planes, the polaron density will fall. Ultimately we end up with total localization of the W^{5+} ions in the *CS* plane, no mobile charge carriers at all, and an insulating oxide. This corresponds to the model used for our earlier electrostatic calculations (*6*). For the purpose of the calculations here, we will assume that the former situation holds, that is, that all or almost all of the W^{5+} states are in the inter-*CS*-plane region of the crystals to produce the highest possible polaron density for any particular degree of reduction.

This polaron population introduces three terms in the free-energy function of the crystal. These are (i) the formation energy of the polarons, (ii) the polaron–polaron interactions, and (iii) polaron–*CS* plane interactions. Of these terms, we have evaluated only (ii) and (iii). Term (ii), polaron–polaron interactions, will be expected to be of greatest importance at high polaron densities, which corresponds to small *CS* plane spacings. Term (iii), polaron–*CS* plane interactions will be of importance at all *CS* plane spacings, but would be expected to dominate term (ii) at large *CS* plane spacings.

2. The Polaron Distribution between *CS* Planes

When one considers the geometry of a *CS* plane, it is seen that the metal to oxygen ratio within the *CS* plane itself falls to a value below that of the WO_3 matrix, 3.0 (see (*1*, *2*) for details). If we consider the *CS* plane to contain only W^{6+} and O^{2-} ions the *CS* plane will now have an overall positive charge per unit area given by $\sigma_0 e$, where e is the charge on the electron and σ_0 is given by Eq. (1) for a $\{10m\}$ *CS* plane;

$$\sigma_0 = \frac{2(2)^{1/2}(m-1)}{[(m-1)^2+(m+1)^2]^{1/2}} \frac{1}{a^2}. \quad (1)$$

In this equation a is the lattice constant of the idealized cubic WO_3 structure, which is equal to an octahedron diagonal, approximately 0.38 nm. If we wish to assume that not all of the charge is distributed in this way, but some W^{5+} ions exist in the *CS* plane we can formally adopt the device of making the value of e tend towards zero.

Because the polarons are effectively negatively charged and the *CS* planes positively charged, there will be a net attraction

between polarons and the *CS* planes. The polarons will therefore not be distributed evenly in the inter-*CS*-plane region, but will tend to aggregate in the regions near to the *CS* planes, creating a high-density region and leaving a low density of polarons midway between the *CS* planes. This is shown schematically in Fig. 1. We also assume that this polaron distribution shields the *CS* planes from one another, so that electrostatic interactions of the sort described in (6) can be neglected.

The positive charge on the *CS* planes will give rise to a potential in the inter-*CS*-plane region. Thus the potentials due to two adjacent *CS* planes in an array of $\{10m\}$ *CS* planes, denoted by *CS* 1 and *CS* 2 can be estimated by classical electrostatic formulas. In doing this though, we will assume that these potentials are shielded by the polaron population in the vicinity of the *CS* planes *CS* 1 and *CS* 2, and so we introduce a shielding constant, K, into the equations. We can therefore write the potentials due to *CS* 1 and *CS* 2, V_1 and V_2 respectively, as

$$V_1 = (\sigma_0 e\lambda^*/4\pi\epsilon_0)e^{-K(r+d/2)}, \quad (2)$$

$$V_2 = (\sigma_0 e\lambda^*/4\pi\epsilon_0)e^{K(r-d/2)}, \quad (3)$$

where we refer to the coordinate axes shown in Fig. 1, and d is the spacing between *CS* 1 and *CS* 2, λ^* is the strength constant, defined further below, K is the screening constant, r is the distance from the origin, midway between the *CS* planes, and $\sigma_0 e$ the surface charge per unit area on *CS* 1 and 2, as defined above. The quantity $4\pi\epsilon_0$ appears as we are working in SI units. The value of the screening constant has to be estimated, and for physical reasons it is reasonable to chose a value about equal to the reciprocal of the polaron radius r_p.

The resultant potential V, due to *CS* 1 and *CS* 2 is given by

$$\begin{aligned} V &= V_1 + V_2 \\ &= (\sigma_0 e\lambda^*/4\pi\epsilon_0)e^{-Kd/2}(e^{-Kr} + e^{Kr}) \\ &= (\sigma_0 e\lambda^*/2\pi\epsilon_0)e^{-Kd/2}\cosh(Kr). \end{aligned} \quad (4)$$

These potentials are shown schematically in Fig. 2.

The next task is to estimate the distribution of the polarons in the inter-*CS*-plane region. As explained, this distribution will not be uniform due to interaction with the

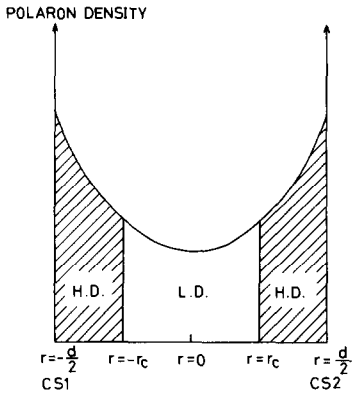

FIG. 1. Schematic illustration of the variation in polaron density between two $\{10m\}$ *CS* planes, *CS* 1 and *CS* 2, separated by a distance d. The regions L.D. and H.D. refer to low-polaron-density and high-polaron-density regions, the change coming at a distance $r = \pm r_c$. The origin of the coordinate system for the calculations is taken as midway between the *CS* planes.

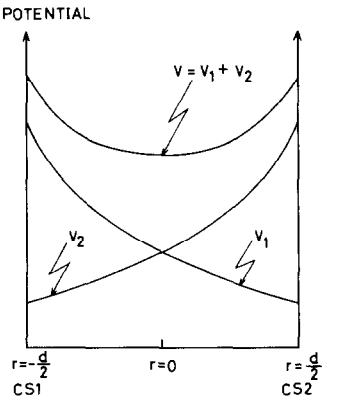

FIG. 2. Schematic illustration of the variation of the potentials V_1, V_2, and $V = V_1 + V_2$ due to two $\{10m\}$ *CS* planes in an array of $\{10m\}$ *CS* planes separated by a distance d.

overall positive charge which we have taken to exist on the *CS* planes. We assume that the polarons are distributed in tunnels of unit area separating the *CS* planes. In reality the polarons are localized at cation sites, but this does not significantly change the theoretical arguments, and in this way we can obtain the density of carriers by use of Poisson's equation:

$$\rho = -\epsilon_0 \nabla^2 V$$
$$= -(\sigma_0 e\lambda^*/2\pi)e^{-Kd/2}K^2 \cosh(Kr). \quad (5)$$

We can make further use of this equation. We know that reduced crystals will be electrically neutral overall, that is, the net charge on the *CS* planes must balance the polaron charges between the *CS* planes. Using this neutrality condition we can determine the strength constant, λ^* from the equation

$$\sigma_0 e + 2\int_0^{d/2} \rho\, dv = 0, \quad (6)$$

where dv is a volume element, $s \times dr$, s being the cross-sectional area of the tunnel containing the polarons which we take as unity to agree with the units of charge per unit area on the *CS* planes. From Eq. (6) we find

$$\lambda^* = (\pi/K)e^{Kd/2}[\sinh(\tfrac{1}{2}Kd)]^{-1}, \quad (7)$$

and substituting from Eq. (7) we can rewrite Eq. (4) and (5) as

$$V = (\sigma_0 e/2K\epsilon_0)[\sinh(\tfrac{1}{2}Kd)]^{-1}\cosh(Kr), \quad (4')$$

$$\rho = -(\sigma_0 eK/2)[\sinh(\tfrac{1}{2}Kd)]^{-1}\cosh(Kr). \quad (5')$$

The Polaron Theory that we have followed is that of Masumi (*16, 17*) and we have taken the case of intermediate polaron coupling. In this case, as investigated in other materials (*15*), the coupling constant, α, is taken as being somewhat greater than unity, and probably in the range $4 > \alpha > 1$. In this case, according to Masumi (*16*), the charge on a polaron, which we can write as $-\sigma_p e$, will be given by

$$\sigma_p e = e - \left[\frac{1}{\kappa_\infty} - \frac{1}{\kappa_0}\right] e, \quad (8)$$

where κ_∞ and κ_0 are the optical and static dielectric constants for WO_3. The values we have taken are those given by Salje (*8*); i.e.,

$$\kappa_\infty \simeq 6.02, \qquad \kappa_0 \simeq 7.9\text{–}9.8.$$

Taking an average value for κ_0 we find

$$\sigma_p e = 0.95e. \quad (9)$$

These terms refer to stoichiometric WO_3. In order to be strictly correct we should, of course, use dielectric-constant data pertinent to reduced WO_3. These values are likely to be much higher than the values used, especially at higher temperatures. However, the results presented later will all be moved by similar amounts by any such change, and comparisons such as we will present will not be seriously effected. Because of this we have not bothered to repeat the calculations for a variety of dielectric-constant values.

Using the equations above, we can finally write

$$\rho_p = \rho/(-\sigma_p e) = (\sigma_0 K/2\sigma_p)[\sinh(\tfrac{1}{2}Kd)]^{-1}\cosh(Kr)$$
$$= \psi \cosh(Kr), \quad (10)$$

where

$$\psi = (\sigma_0 K/2\sigma_p)[\sinh(\tfrac{1}{2}Kd)]^{-1}. \quad (11)$$

3. The Interaction between Polarons and *CS* Planes, E_{s-p}

This potential energy term is due to the interaction of a polaron at r with the potential V from *CS* planes *CS* 1 and *CS* 2, which we write as U_{s-p}. This is simply given by

$$U_{s-p} = V(-\sigma_p e). \quad (12)$$

The total potential energy of all the polarons within the tunnel of unit area lying between *CS* 1 and *CS* 2 will therefore be given as E_{s-p}, where

$$E_{s-p} = s\int_0^{d/2} U_{s-p}\cdot\rho_p\cdot dr$$

$$= -\frac{(\sigma_0 e)^2}{8\epsilon_0}[\sinh(\tfrac{1}{2}Kd)]^{-2}\left[\frac{\sinh(Kd)}{K} + d\right]. \quad (13)$$

4. The Polaron–Polaron Interaction, E_{p-p}

4.1. General

The interaction energy between two polarons will clearly depend upon their separation. The form that this interaction will take is difficult to express analytically, but relatively easy to describe qualitatively. At low polaron densities the interaction will be small, and will increase smoothly as the polaron separation decreases, until we reach the stage where we can consider ourselves to be in the high-density region. If a further decrease in interpolaron separation is envisaged the interaction would be expected to increase steeply through a dense packing regime to a hard core. In this latter case we are effectively trying to superimpose polarons to produce W^{4+} states, which we assume to require prohibitively high energies in the present analysis. We have shown this qualitative form of the interaction energy in Fig. 3a.

As described earlier, the region between *CS* planes can be divided into a low-polaron-density region, roughly speaking midway between the *CS* planes, and a high-polaron-density region in the neighborhood of the *CS* planes. Analytical forms for the interaction energy between two polarons, U_{p-p}, for these two regions, have been given by Masumi (*16*) as

$$U_{p-p}(\mathrm{HD}) = A\exp(-2R/r_p)$$

$$0 \le R \le R_c \text{ (high density)}, \quad (14)$$

$$U_{p-p}(\mathrm{LD}) = \frac{\alpha}{4\pi\epsilon_0}\frac{(-\sigma_p e)^2}{R}$$

$$R \le R_c \text{ (low density)}, \quad (15)$$

where R is the interpolaron distance as

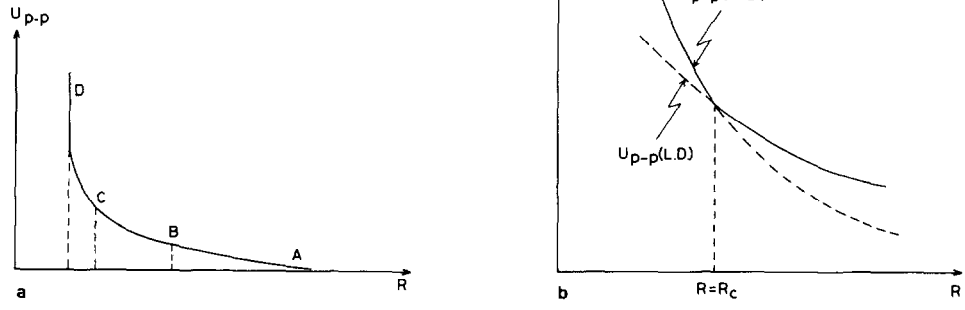

FIG. 3.(a) Idealized representation of the polaron–polaron interaction potential, U_{p-p}, for two polarons vs interpolaron spacing, R. A corresponds to the low-polaron-density region, B to the high-density region, C to a dense-packing regime, and D to the hard-core region which physically corresponds to the formation of W^{4+} ions. (b) A more detailed illustration of the interaction potentials used in our calculations for the regions of low (L.D.) and high (H.D.) polaron densities. At $R = R_c$ the form of the interaction changes in accordance with Eqs. (14) and (15).

used by Masumi, r_p is the polaron radius, and R_c is the interpolaron distance at which the low-density interaction changes to the high-density interaction. These interactions are shown in Fig. 3b from which it can be seen that the interaction in the high-density region is much stronger than that in the low-density region in the range of $R \leq R_c$.

In considering Fig. 3b we notice a discontinuity between the low-density region and the high-density region which occurs at $R = R_c$. This discontinuity is, of course, due to using Eq. (14) and (15) in too rigid a manner, and in reality a smooth transition from one region to the other, as shown in Fig. 3a, will surely occur in practice. The term R_c therefore has no precise meaning in physical terms, but will be retained as useful in delineating the extent of the high- and low-density regions.

If we compare Fig. 3 with Fig. 1 we see that R_c in Fig. 3b corresponds to $r = \pm r_c$ in Fig. 1, and furthermore that the region $|r| \leq r_c$ corresponds to the low-density region and the area $r_c \leq |r| \leq d/2$ contains high-density polarons. In addition, at $r = \pm r_c$, R is equal to R_c, and hence the following relation must be satisfied.

$$A \exp\left(\frac{-2R_c}{r_p}\right) = \frac{\alpha}{4\pi\epsilon_0} \frac{(-\sigma_p e)^2}{R_c} \quad (16)$$

so that the constant A is given by Eq. (17):

$$A = \frac{\alpha}{4\pi\epsilon_0} \frac{(-\sigma_p e)^2}{R_c} \exp\left(\frac{2R_c}{r_p}\right). \quad (17)$$

We can also relate the interpolaron distance, R, to the polaron density ρ_p, given earlier, by the simple relationship

$$R = \rho_p^{-1/3}. \quad (18)$$

To express this in terms of the other variables in Eqs. (10) and (11) we introduce a function ϕ, given by

$$\phi = \psi \sinh(Kr), \quad (19)$$

then

$$d\phi = K[\psi \cosh(Kr)]dr = K\rho_p dr;$$

i.e.,

$$\rho_p dr = (1/K)d\phi \quad (20)$$

and

$$R = \rho_p^{-1/3} = [(\phi^2 + \psi^2)^{1/2}]^{-1/3} = (\phi^2 + \psi^2)^{-1/6}. \quad (21)$$

We can now write expressions for the total polaron interactions in the inter-CS-plane regions of the crystal. Firstly, for the high-density region, we find the total interaction E_{p-p} (high) is given by

$$\begin{aligned} E_{p-p}(\text{high}) &= 2\int_{r_c}^{d/2} U_{p-p} \cdot \rho_p \cdot dr \\ &= (2/K)\int_{\phi_c}^{\phi_d} U_{p-p} d\phi \\ &= 2A/K \int_{\phi_c}^{\phi_d} \exp\left[-\frac{2(\phi^2 + \psi^2)^{-1/6}}{r_p}\right] d\phi, \end{aligned} \quad (22)$$

where

$$\phi_d = [\psi \sinh(Kr)]_r = d/2 = \psi \sinh(\tfrac{1}{2}Kd), \quad (23)$$

$$\phi_c = [\psi \sinh(Kr)]_r = r_c = (R_c^{-6} - \psi^2)^{1/2}. \quad (24)$$

It is impossible to solve the integral in Eq. (22) algebraically, but it can be evaluated numerically using a computer.

In the low-density region, the total polaron–polaron interaction, E_{p-p} (low), is given as

$$\begin{aligned} E_{p-p}(\text{low}) &= 2\int_0^{r_c} U_{p-p} \cdot \rho_r \cdot dr \\ &= 2\alpha(-\sigma_p e)^2/4\pi K\epsilon_0 \int_0^{\phi_c} (\phi^2 + \psi^2)^{-1/6} d\phi. \end{aligned} \quad (25)$$

Thus we can write the total polaron–polaron interaction, E_{p-p} as the sum of E_{p-p}

(high) and E_{p-p} (low); i.e., the sum of Eqs. (22) and (25).

4.2. Estimation of Polaron Density

In the previous section we considered a high-density and a low-density polaron region between *CS* planes *CS* 1 and *CS* 2. Clearly the extent of these two regions will depend upon the polaron radius and whether we assume that polarons can overlap or not. It is not easy to estimate the polaron radius. According to Masumi (*17*), however, it is reasonable that the polaron radius has a value larger than the spacing between cations. As the distance between the nearest cation sites in WO_3 is about 0.38 nm, it would seem reasonable to consider the polaron radius to lie in the range from 0.2 to 1 nm.

We can also make an independent estimate of the polaron radius by considering the carrier densities in reduced WO_3 crystals. To do this, we assume that each oxygen atom lost contributes two mobile charge carriers. We may then proceed as follows:

(i) We know that W^{4+} states do not occur in these crystals and this indicates a very high formation energy for electronic entities such as bipolarons with two electrons at the same lattice site. We can therefore suggest that the minimal polaron–polaron distance will be the W–W distance in WO_3, with a polaron centred upon each metal atom. As the tungsten atoms are separated by about 0.38 nm we would thus have a polaron radius of about 0.19 nm. If each tungsten atom acts as a polaron site, i.e., they are all formally in the W^{5+} state, the carrier density will be a maximum at 1.8×10^{22} cm^{-3} and the composition will be W_2O_5, i.e., $WO_{2.5}$.

(ii) From this most closely packed stage we can imagine other polaron distributions that are more open. For example, if polarons are located on every other tungsten atom along two of the unit cell diagonal 110 directions of the idealized cubic unit cell, they can be allocated a disk shape of about 1.1 nm diameter and 0.38 nm in thickness. This will give a maximum density of about 2×10^{21} charge carriers/cm^3 in crystals with an overall composition of about $WO_{2.88}$.

(iii) If we assume that the polarons are spherical, and occupy every other tungsten position along all of the ⟨110⟩ directions of the idealized cubic unit cell of WO_3, they will have about 1.1 nm diameter. Closest packing of these polarons will lead to a carrier density of about 6.7×10^{20} cm^{-3} in crystals of composition about $WO_{2.90}$.

This latter value is in fairly good agreement with observed carrier concentrations in WO_{3-x} crystals. We can suggest, therefore, that a reasonable polaron radius in these reduced oxides is about 0.55 nm. Once again, therefore, a choice of polaron radius in the range 0.2–1.0 nm would seem to cover all reasonable possibilities, and we are led to the conclusion that for all but the smallest degrees of reduction, polarons of these radii will be fairly densely packed.

We can illustrate this in the following way. Let us consider the larger of these values, i.e., r_p, the polaron radius, = 1 nm. If we assume that polarons do not overlap, then clearly the spacing between *CS* 1 and *CS* 2 must have a minimum of approximately 2 nm. This corresponds to n values of about 13 for {102} *CS* planes, $n = 18$ for {103} *CS* planes and $n = 6$ for {001} *CS* planes, where n is an integer in the series formula W_nO_{3n-m+1}, which represents the compositions available to a crystal containing an ordered array of $\{10m\}$ *CS* planes (*1, 2*). We can also note that in such cases there is only room for one polaron in the tunnel of unit area that we are considering and hence we have no polaron–polaron interaction within the tunnel to contend with. This would seem to be unreasonable, so we will suppose that the polarons do overlap one another to some extent and we

are lead to the conclusion that the whole of the matrix between *CS* planes *CS* 1 and *CS* 2 must be considered as a high-density region.

We can consider the interpolaron spacing in a more quantitative way by making use of Eqs. (18) and (10). To do this, however, it is necessary to include a value for the screening length, $1/K$. Earlier it was suggested that a value of $1/K$ approximately equal to the polaron radius would be appropriate, and hence we have chosen values for the screening length, $1/K$, to range from 0.2 to 1 nm. To make the estimate we have also considered *CS* plane arrays with n taking values of from 6 to 34 for {102} *CS* planes, 9 to 46 for {103} *CS* planes, and from 3 to 17 for {001} *CS* plane arrays. Putting the *CS* plane spacings, d, into Eq. (10) and also substituting a value of $r = 0$, yields a minimum value for ρ_p, which from Eq. (18) allows us to calculate a maximum value for the interpolaron spacing, R_{max}. A similar procedure is used to calculate the minimum polaron separation, R_{min}. In this case we use $r = d/2$ instead of $r = 0$ in Eq. (10). The results are given in Table I. From these values, the case of an R_{max} of 44.5 nm for $1/K = 0.2$ nm seems to be anomalously large, therefore in further calculations we have only employed $1/K$ values of from 0.4 to 1.0 nm.

TABLE I

THE MAXIMUM (R_{max}) AND MINIMUM (R_{min}) VALUES OF THE POLARON SPACING BETWEEN *CS* PLANES IN {102}, {103}, AND {001} ARRAYS FOR VALUES OF THE SCREENING CONSTANT, K, SPECIFIED, AND MAXIMUM POSSIBLE VALUES OF THE POLARON RADIUS, $r_{p_m max}$ CALCULATED FROM EQ. (27)

$1/K$ (nm)	R_{max} (nm)	R_{min} (nm)	$r_{p_m max}$ (nm)
0.2	44.5	0.2	16.4
0.4	4.1	0.3	2.9
0.6	2.0	0.3	1.8
0.8	1.4	0.3	1.4
1.0	1.2	0.3	1.3

As it would seem reasonable to consider the whole of the matrix between the *CS* planes as a high-polaron-density region, we can also write, in the limits $R_{min} > R > R_{max}$,

$$A \exp\left(\frac{-2R}{r_p}\right) > \frac{\alpha}{4\pi\epsilon_0}\frac{(-\sigma_p e)^2}{R}. \quad (26)$$

This can be considered to be equivalent to the assumption $R_c = R_{max}$ and is shown diagrammatically in Fig. 4. In reality this condition is somewhat of a mathematical fiction but even so it has some measure of usefulness and is worth retaining as a simplifying approximation.

From Eqs. (26) and (17), we can now write

$$\frac{\alpha(-\sigma_p e)^2}{4\pi\epsilon_0}\frac{1}{R_{max}} \exp\left(\frac{2R_{max}}{r_p}\right)\exp\left(\frac{-2R_{min}}{r_p}\right) > \frac{\alpha(-\sigma_p e)^2}{4\pi\epsilon_0}\frac{1}{R_{min}};$$

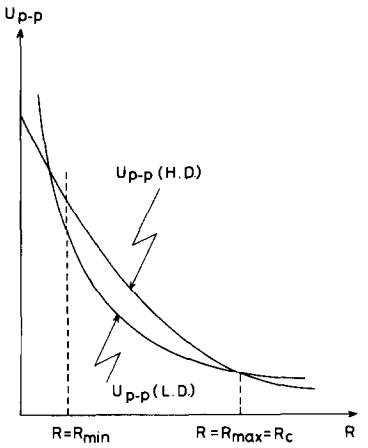

FIG. 4. Schematic illustration of the model for polaron distribution used in the present calculations. All of the inter-*CS* matrix is considered to be a high-polaron-density (H.D.) region, which persists to $R_{max} \equiv R_c$. Curve U_{p-p} (HD) represents the term $A \exp(-2R/r_p)$ and curve U_{p-p} (LD) the term $[\alpha/4\pi\epsilon_0][(-\sigma_p e)^2/R]$ in Eq. (26).

hence

$$\frac{2(R_{max} - R_{min})}{r_p} > \ln\left(\frac{R_{max}}{R_{min}}\right)$$

and

$$\frac{2(R_{max} - R_{min})}{\ln(R_{max}/R_{min})} = r_{p_{max}} > r_p. \quad (27)$$

This means that the polaron radius, r_p, must always be less than $r_{p_{max}}$. The value of $r_{p_{max}}$ is readily obtained from the data already given in Table I and is also included in Table I. It is seen that the values of the screening length, $1/K$, and polaron radius, r_p, that we will use, 0.4 to 1.0 nm satisfy Eq. (27) and provide further verification that the inter-*CS*-plane region is best treated as a high-density polaron region is the most suitable model to adopt.

The purpose of the considerations in this section has been to try to determine the most realistic situation holding in the *CS* phases. The arguments presented thus suggest that we should only consider the high-density equations when calculating the polaron–polaron interaction E_{p-p}. We can therefore return to the Eqs. (18) to (24). Equations (18) to (21) remain unchanged. The form of Eq. (22) also remains the same, but the limits of the integration are changed so that we write

$$\begin{aligned} E_{p-p} &= 2\int_0^{d/2} U_{p-p}\cdot\rho_p\cdot dv = 2\int_0^{d/2} U_{p-p}\cdot\rho_p\cdot dr \\ &= (2/K)\int_0^{\phi(r=d/2)} U_{p-p}\,d\phi \\ &= \frac{2A}{K}\int_0^{\phi(r=d/2)} \exp\left[\frac{-2(\phi^2+\psi^2)^{-1/6}}{r_p}\right] d\phi. \end{aligned} \quad (28)$$

As we mentioned in conjunction with Eq. (22), Eq. (28) has been evaluated numerically by computer.

5. Total Polaron Interaction Energy

The total polaron interaction energy will now be the sum of the polaron–*CS* plane interaction energy, detailed in Section 3, and the high-density-region polaron–polaron interaction energy detailed in Section 4 above. We can therefore write for the total interaction energy, E_{total},

$$E_{total} = E_{s-p} + E_{p-p}, \quad (29)$$

where E_{s-p} is given by Eq. (13) and E_{p-p} by Eq. (28). E_{total} has been estimated by computer for various degrees of reduction of WO_3.

6. The Polaron Formulation Employed

The majority of the preceding theory has been of general validity, and not bound to any particular choice of polaron theory. However, at two points, which are (a) estimating the charge on the polaron, Eq. (8), and (b) estimating the polaron–polaron interaction, Eqs. (14) and (15), we have chosen to use the Feynman–Masumi model for polaron behavior and taken the equations directly from Masumi's paper (*16*). As the Masumi paper is concerned with polaron dynamics, while the present study considers only static interaction energies, it may be queried as to whether this is reasonable. Let us consider Eqs. (14) and (15) first. In our model we ideally need to reproduce the interaction curve shown in Fig. 3a. Equations (14) and (15) are, in fact, only an approximation to that curve, but we consider them to be an adequate approximation in the context of the present study. When we consider the use of Eq. (8) there are similar difficulties and a number of factors need to be balanced against one another.

Our main consideration is that it is necessary to obtain an estimate of the charge on the polaron. While Masumi's equation which we have used as Eq. (8) may not be altogether ideal for our use it is the best theoretical relationship we have found in the literature. Rather than invent an alternative, it seemed reasonable to use Eq. (8) as it stands in the context of the present calculations.

Finally we should draw attention to the fact that Masumi's study is concerned with large polarons, rather than the small polarons which probably exist in slightly reduced WO_3. Our calculations, though, cover a range of polaron radii which encompass small, medium, and large polarons and which, using Masumi's criterion that the polaron radius should be larger than the cation separation, mostly fall into the large-polaron group. Moreover, it was found that the extension of the equation from the large regions toward smaller polaron radii presented no inconsistencies in the results, but smooth trends resulted, as described below.

In conclusion, we can reiterate that our study is, in effect, an exploratory treatment of polaron interaction energies in reduced tungsten trioxide. At this stage in the investigation, it seemed reasonable to adopt the analytical forms of the Masumi equation, although they apply to large-polaron dynamics, rather than to derive new alternatives. The results reported below, support this decision by showing that in the main polaron interaction energies are rather small compared to other interactions, and even severe changes in the forms of Eqs. (8), (14), and (15) are unlikely to reverse this overall result.

Results and Discussion

Various values of the total polaron interaction energy per unit volume, which is obtained by dividing E_{total} by d, have been calculated. The units used are electron volts per cubic nanometer (eV nm^{-3}), where 1 eV = 1.602×10^{-19} J, and the calculations have been made as a function of the degree of reduction of the tungsten trioxide crystals, x in WO_x. In general, x lies in the range of 2.70 to 3.0, specifying the oxides $WO_{2.70}$ to WO_3. In practice the *CS* phase range for the tungsten oxides only extends to about $WO_{2.85}$, and the composition region below this must be regarded as showing trends rather than applying to real systems. The calculations have been made for four values of the screening length, $1/K$, 0.4, 0.6, 0.8, and 1.0 nm and values of the polaron radius r_p of 0.6, 0.8, and 1.0 nm, which seem reasonable when the data in Table I are consulted. The results are shown in Figs. 5, 6, 7, and 8.

We will begin by considering the overall form of the curves shown in Figs. 5–8 rather than their numerical values. It is apparent that there is a considerable change as we pass from Fig. 5 to Fig. 8. If we look at Fig. 5, we see that the interaction energy increases smoothly as the degree of reduction of the crystal, x, decreases. Moreover, the value of E_{total} is seen to be positive. This indicates that the polaron–polaron interaction, E_{p-p}, is dominant, because E_{p-p} is a positive term in the equation for E_{total}. In Figs. 7 and 8 we see that E_{total} is now negative and, moreover, decreases as the degree of reduction increases. This indicates that in these figures E_{s-p} is dominant as E_{s-p} is a negative term in the equation for E_{total}.

We therefore see that as the polaron screening length increases the interaction changes from being principally polaron–polaron at small screening lengths to mainly polaron–*CS* plane interactions at large screening lengths. We can also see that the value chosen for the polaron radius r_p does not change this conclusion. Certainly the value of the polaron radius changes the magnitude of E_{total} but not the overall trend.

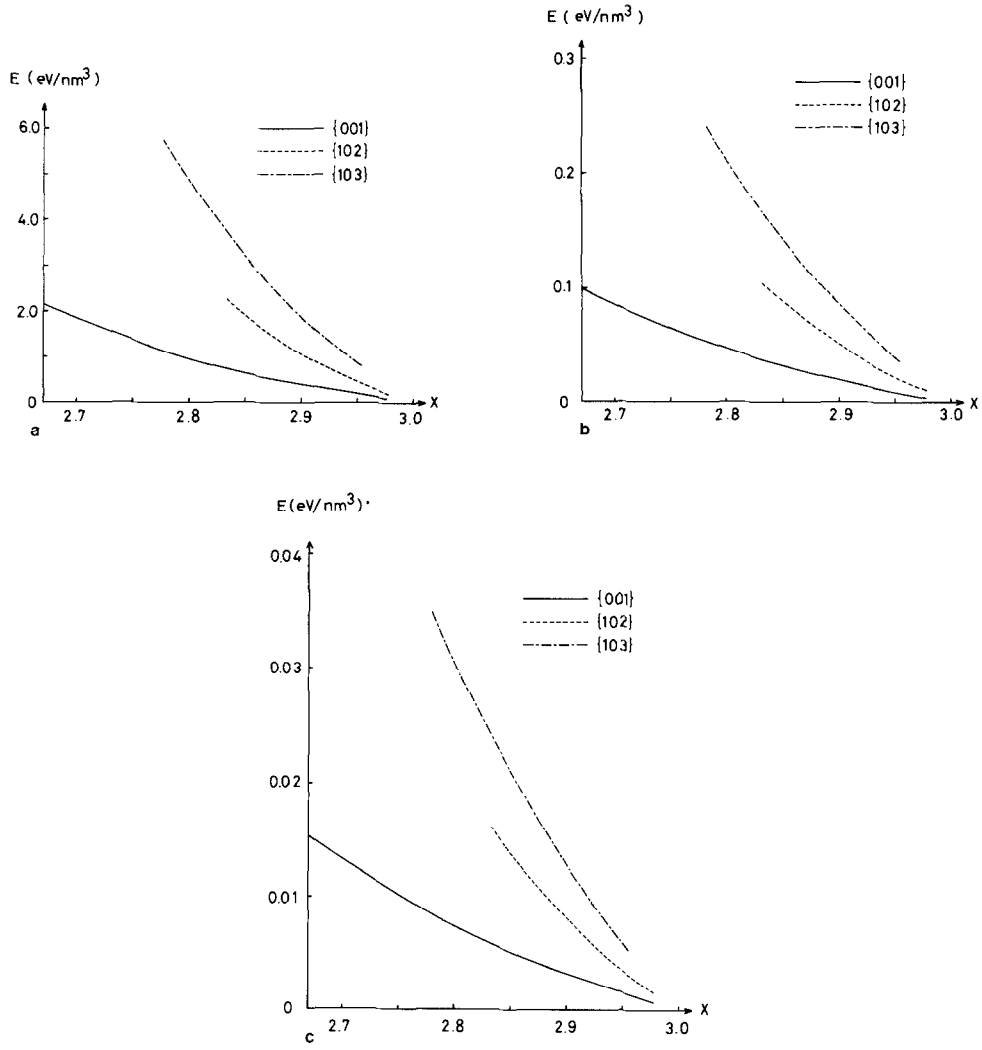

FIG. 5. Total polaron interaction energy per unit volume E (eV/nm^3) versus degree of reduction x in WO_x for a screening length of $1/K = 0.4$ nm and polaron radii, r_p, of (a) 0.6 nm, (b) 0.8 nm, and (c) 1.0 nm.

Thus we find that a small degree of screening allows the polarons to see each other clearly while large screening distances cause the polarons to see the *CS* planes. This suggests that *CS* planes may not act as a barrier to the movement of polarons when the screening length is small and that they may be able to move relatively freely through the crystal, endowing it with a quasi-isotropic electronic conductivity. When the screening length is large, though, polarons will interact with the *CS* planes and it is likely that their movement normal to *CS* planes would be impeded compared to that parallel to the *CS* planes. Hence electronic conductivity would be expected to be noticeably anisotropic. Of course the degree to which these polarons are aware of the *CS* planes will depend upon the overall magnitude of the interaction energy. For

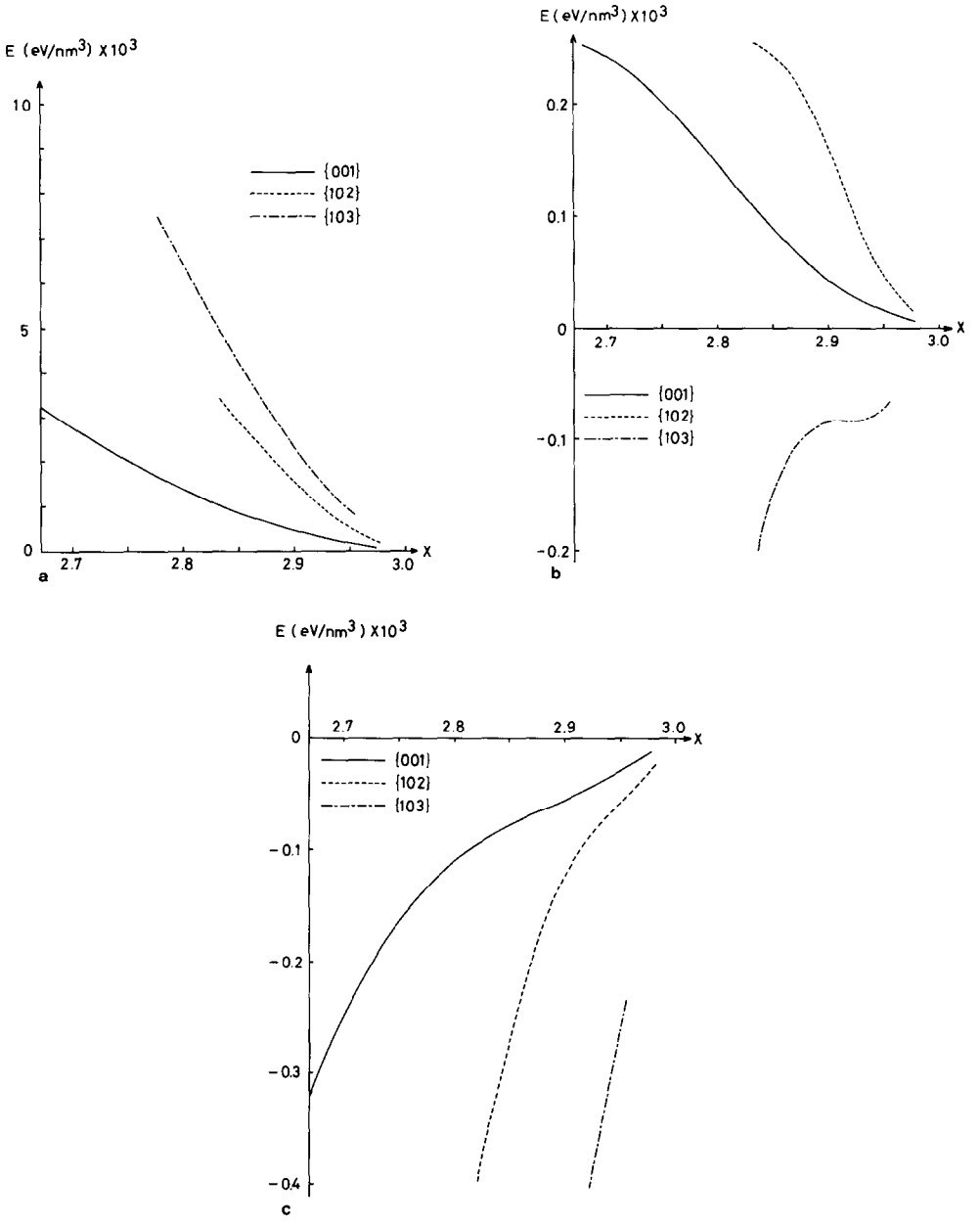

FIG. 6. Total polaron interaction energy per unit volume E (eV/nm^3) versus degree of reduction x in WO_x for a screening length of $1/K = 0.6$ nm and polaron radii, r_p, of (a) 0.6 nm, (b) 0.8 nm, and (c) 1.0 nm.

small values of this interaction energy the degree of impedence may in fact be rather small. It is also noticeable that this behavior is relatively insensitive to the polaron radius chosen, but depends critically upon the degree of screening assumed to be present.

The change from the polaron–*CS* plane

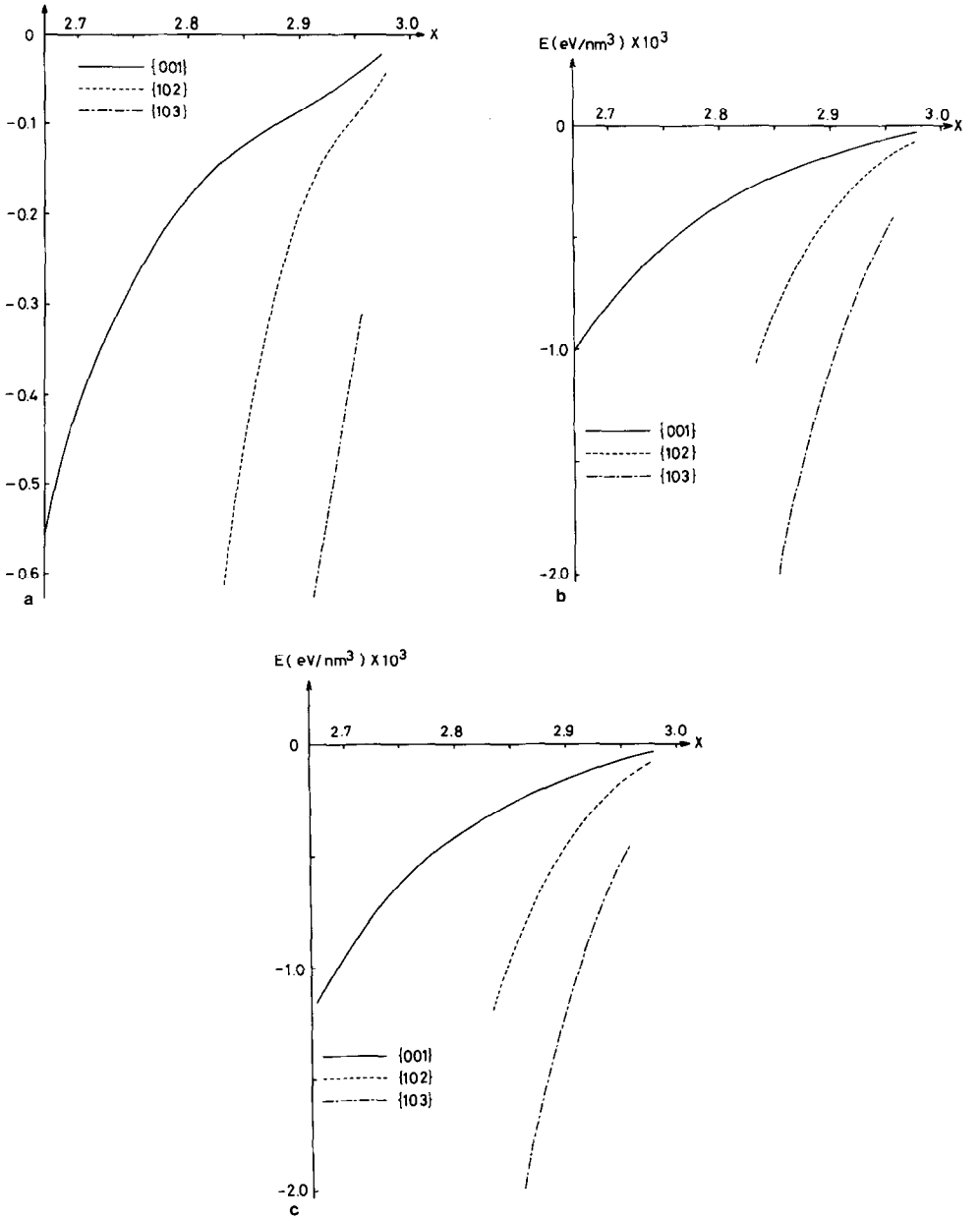

FIG. 7. Total polaron interaction energy per unit volume E (eV/nm^3) versus degree of reduction x in WO_x for a screening length of $1/K = 0.8$ nm and polaron radii, r_p of (a) 0.6 nm, (b) 0.8 nm, and (c) 1.0 nm.

interaction dominant region to the polaron–polaron interaction dominant region occurs for a screening length of $1/K = 0.6$ nm, illustrated in Fig. 6. In this case the interactions are very delicately balanced, so that not only is the total interaction energy dependent upon polaron radius, but also upon *CS* plane type. Thus we see that for

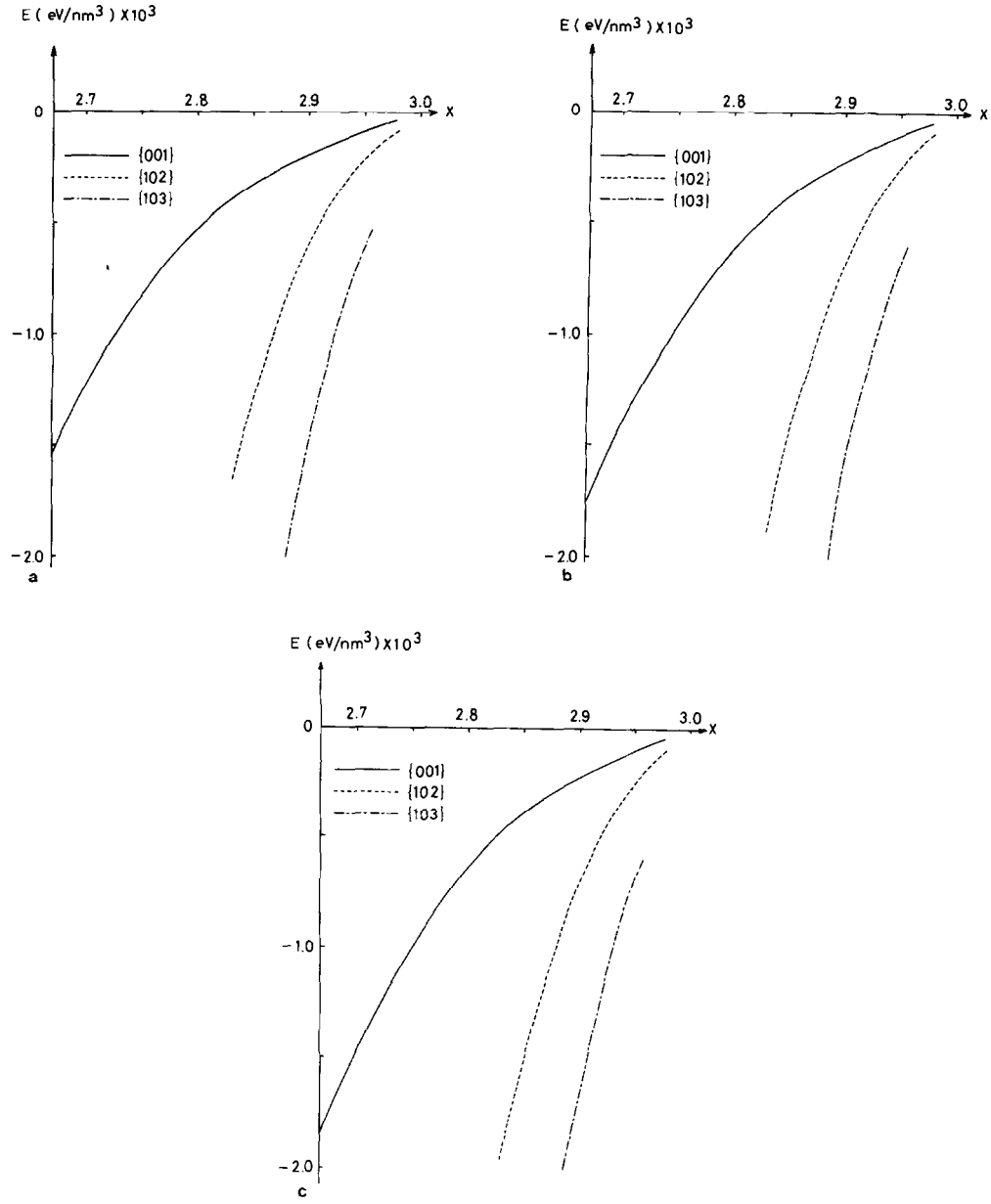

FIG. 8. Total polaron interaction energy per unit volume E (eV/nm^3) versus degree of reduction x in WO_x for a screening length of $1/K = 1.0$ nm and polaron radii, r_p, of (a) 0.6 nm, (b) 0.8 nm, and (c) 1.0 nm.

small polaron radii, i.e., 0.6 nm, the interaction is principally due to polaron–polaron interactions. When the polaron radius reaches 1.0 nm the energy is mainly due to the polaron–*CS* plane interactions. Between these values, at a polaron radius of 0.8 nm the interaction changes from mainly polaron–polaron in the case of {001} and

{102} *CS* plane arrays to mainly polaron–*CS* plane in the case of a {103} *CS* plane array. Clearly if the screening length and polaron radius are allowed to vary freely it would be possible, in this region of values, to make the total polaron interaction energy zero. It must be remembered, however, that it is not an absolute zero for the energy, and crystals with a total negative energy will be more stable than ones with zero energy.

We see from Figs. 5–8 that the overall shape of the interaction energy curves are rather critically dependent upon the degree of screening but insensitive to the polaron radius used. When we come to consider the magnitude of the interaction we see that the polaron radius, r_p, plays a larger role. In Fig. 5 we see that as the polaron radius increases the interaction energy decreases. This trend is actually due to the following two reasons. Firstly, both polaron–polaron and polaron–*CS* interactions weaken as the polaron radius increases so that the magnitude of these energies becomes smaller. Secondly, we have an increase in the polaron–*CS* plane interaction at the expense of the polaron–polaron interaction. Thus increasing polaron radius causes the negative polaron–polaron interaction to become more dominant. This trend is seen in all the remaining curves of Figs. 6 to 8. Hence in Fig. 8 we see that the total interaction energy becomes more negative as the polaron radius increases, in accord with Fig. 5.

The magnitude of the interaction also varies with the screening length $1/K$. When $1/K$ is smallest, 0.4 nm, the interaction energy is very large, particularly for small polaron radii. The values are in fact so large as to make them of great importance in any energy scheme for *CS* phases. We do not have any experimental evidence to show whether such interaction energies are realistic and it would be of some interest to investigate this further. When the screening length increases we find that the interaction energy becomes small and hardly varies significantly with either screening length or polaron radius.

We can summarize these results thus:

(i) The degree of screening of the polarons from the *CS* planes, represented by the screening length, $1/K$, in our calculations, is of prime importance in controlling the interaction energy. As the screening length increases the total interaction falls, but we find only very small changes for screening lengths much more than 0.6 nm. We also find that as the screening length increases the interaction changes from being dominated by polaron–polaron interactions, which are positive, to polaron–*CS* plane interactions, which are negative.

(ii) The polaron radius is not so critical as the screening length, but we find that as the polaron radius increases the polaron–*CS* plane interaction increases in importance compared to the polaron–polaron interaction.

Having discussed the general nature of the results and their dependence on the numerical parameters, we can now turn to the question of the extent to which these polaron interaction energies are likely to influence or control the microstructures of the WO_3-related *CS* phases.

Initially let us consider the results shown in Fig. 5. In this case the interaction energies are high, particularly for a polaron radius of 0.6 nm. As such, they are at least comparable to *CS* plane formation energies (*3*) and so, if these conditions held in practice, we would expect them to dominate *CS* plane microstructures. We note from Fig. 5 that {001} *CS* phases are those with the lowest interaction energy, and hence {001} *CS* planes would be expected to occur in practice. This is not so, as {102} *CS* planes form on initially reducing WO_3, and these give way to {103} *CS* planes at compositions below about $WO_{2.94}$. We also note, from the data shown in Fig. 5, that the

change from {102} *CS* to {103} *CS* arrays will actually increase the interaction energy. Hence we feel that the polaron radius and small screening length combination shown in Fig. 5 does not hold in real crystals, as the magnitudes of the interaction energy terms do not agree with observations.

When we consider the magnitudes of the total polaron interaction energies for the combination of screening lengths and polaron radii shown in Figs. 6–8, we find them to be fairly small. Elastic strain energy interactions calculated previously (*1–3*) are considerably higher for similar composition ranges. It therefore seems reasonable to suppose that polaron interactions in both the low-density and high-density regions investigated here will not influence *CS* phase microstructures significantly. We can also note that for most of the situations investigated, {103} *CS* arrays have a lower polaron interaction energy than {102} *CS* arrays. Thus, for a crystal of any particular composition a change from a {102} microstructure to a {103} microstructure will result in a gain in energy. This is a similar situation to that found for elastic strain energies, and as such we would expect the polaron interactions to reinforce the trend given by the elastic strain calculations.

The changes in interaction energy with *CS* plane type can be viewed in another way. It was pointed out above that in Fig. 5 polaron–polaron interactions are dominant, whereas in Figs. 8 and 9 polaron–*CS* plane interactions come to the fore. Hence, if polaron–polaron interactions are more important, {102} *CS* planes are preferred over {103} *CS* planes, and this preference will become more apparent as the degree of reduction increases. Similarly, though, if the polaron–*CS* plane interaction dominates, {103} *CS* planes will be preferred, and again this preference will become more pronounced as the degree of reduction increases. It is possible to conceive that at low-*CS*-plane densities polaron–polaron interactions will predominate and that at high-*CS*-plane densities polaron–*CS* plane interactions will be more important. This is formally equivalent to the situation shown in Fig. 6, where we change from a state in which {102} *CS* arrays have lower energy than {103} *CS* arrays to that in which {103} arrays are preferred.

We can summarize this section by concluding that:

(i) For most of the low- and high-polaron density regions investigated here, polaron interactions are in general too small to dominate *CS* plane interaction energies and so control *CS* phase microstructures.

(ii) The combination of small polaron radius and screening length, does, however, lead to very high interaction energies. Experimental observations on *CS* plane microstructures suggest that this combination is unlikely to occur in real crystals and it is more likely that polaron interaction will be better represented by larger polaron radii and screening lengths.

Finally, we wish to consider, in a qualitative fashion, some of the consequences of the hard-core type of potential which we have illustrated in Fig. 3a, but which we have not investigated numerically, as we do not have reliable potential functions to employ. In this regime, polaron–polaron interactions are likely to increase rapidly and may well provide the major energy criterion for termination of a *CS* phase series. We can illustrate this by comparing the $(Mo,W)_nO_{3n-1}$ oxides with the binary W_nO_{3n-1} oxides. In the binary oxides, as we have pointed out, charge carrier densities are high, and we clearly have an appreciable polaron density between the *CS* planes. In contrast, the charge carrier densities in $(Mo,W)O_{3n-1}$ are low (*15*), suggesting that Mo^{5+} states are preferred to W^{5+} states, and that they are localized in the *CS* plane. Thus on reduction of the respective series, the binary oxide series will reach a high

polaron density, and approach the hard core potential region at much smaller degrees of reduction than in the ternary molybdenum–tungsten oxides, although both these oxide series are isostructural.

This idea accords well with experimental observations. In the binary system, the W_nO_{3n-1} series persists to about $W_{16}O_{47}$ (i.e., $WO_{2.94}$) before changing to the W_nO_{3n-2} series, which has wider spaced *CS* planes for the equivalent degree of reduction, and hence a lower polaron density. The $(Mo,W)_nO_{3n-1}$ series, however, persists to n values of 10, i.e., $(Mo,W)_{10}O_{29}$ or $(Mo,W)O_{2.90}$, and in the binary molybdenum oxides, to the isostructural Mo_9O_{26} and Mo_8O_{23}. Polaron interactions provide an attractive mode of explaining this difference, as the changes in elastic strain energy which result from a replacement of W^{6+} by Mo^{6+} are likely to be small.

The points in this final section are somewhat speculative as they lie outside the domain of our calculations. Further experimental results and calculations relevant to this regime of polaron–polaron interactions would be of some interest.

Acknowledgments

E.I. is indebted to Professor R. Wada for his encouragement during this work and wishes to thank Mr. H. Kanai and Mr. M. Taiji for their assistance with calculations.

References

1. E. IGUCHI AND R. J. D. TILLEY, *Phil. Trans. Roy. Soc. Ser. A* **286,** 55 (1977).
2. R. J. D. TILLEY, *J. Solid State Chem.* **19,** 53 (1976).
3. E. IGUCHI AND R. J. D. TILLEY, *J. Solid State Chem.* **24,** 121, 131 (1978).
4. E. IGUCHI AND R. J. D. TILLEY, *J. Solid State Chem.* **29,** 435 (1979).
5. E. IGUCHI AND R. J. D. TILLEY, *J. Solid State Chem.* **32,** 221 (1980).
6. E. IGUCHI AND R. J. D. TILLEY, *J. Solid State Chem.* **21,** 49 (1977).
7. J. M. BERAK AND M. J. SIENKO, *J. Solid State Chem.* **2,** 109 (1970).
8. E. SALJE, *Optics Commun.* **24,** 231–232 (1978).
9. E. SALJE AND K. VISWANATHAN, *Acta Crystallogr. Sect. A* **31,** 356 (1975).
10. E. SALJE, R. GEHLIG, AND K. VISWANATHAN, *J. Solid State Chem.* **25,** 239 (1978).
11. G. HOPPMANN AND E. SALJE, *Philos. Mag.*, in press.
12. I. LEFKOWITZ, M. B. DOWELL, AND M. A. SHIELDS, *J. Solid State Chem.* **15,** 24 (1975).
13. B. A. DE ANGELIS AND M. SCHIAVELLO, *J. Solid State Chem.* **21,** 67 (1971).
14. K. VISWANATHAN, K. BRANDT, AND E. SALJE, *J. Solid State Chem.* **36,** 45 (1981).
15. E. SALJE, A. CARLEY, AND M. W. R. ROBERTS, *J. Solid State Chem.* **29,** 237 (1979).
16. T. MASUMI, *Progr. Theoret. Phys. Suppl.* **22**(57) (1975).
17. T. MASUMI, *Solid State Phys.* **8,** 369 (1973). (AGNE, Tokyo; in Japanese).